Electrical characterization of DNA-functionalized solid state nanopores for bio-sensing

2010 J. Phys.: Condens. Matter 22 454104

(http://iopscience.iop.org/0953-8984/22/45/454104)

J. Phys.: Condens. Matter **22** (2010) 454104 (7pp) doi:10.1088/0953-8984/22/45/454104

Electrical characterization of DNA-functionalized solid state nanopores for bio-sensing

V Mussi[1], P Fanzio[1,2], L Repetto[1], G Firpo[1], P Scaruffi[3], S Stigliani[3], M Menotta[4], M Magnani[4], G P Tonini[3] and U Valbusa[1]

[1] Nanomed Labs, Physics Department, University of Genova, and Nanobiotechnologies, National Institute of Cancer Research (IST), Largo R Benzi, 10 Genova, 16132, Italy
[2] Italian Institute of Technology (IIT), via Morego, 30 Genova, 16163, Italy
[3] Translational Pediatric Oncology, National Institute for Cancer Research (IST), Largo R Benzi, 10 Genova, 16132, Italy
[4] Department of Biomolecular Sciences, University of Urbino 'Carlo Bo', Via Saffi 2, 61029 Urbino, PU, Italy

E-mail: mussi@fisica.unige.it

Received 30 March 2010, in final form 4 June 2010
Published 29 October 2010
Online at stacks.iop.org/JPhysCM/22/454104

Abstract
We present data concerning the electrical properties of a class of biosensor devices based on bio-functionalized solid state nanopores able to detect different kinds of interactions between probe molecules, chemically attached to the pore surface, and target molecules present in solution and electrophoretically drawn through the nanometric channel. The great potentiality of this approach resides in the fact that the functionalization of a quite large pore (up to 50–60 nm) allows a sufficient diameter reduction for the attainment of a single molecule sensing dimension and selective activation, without the need for further material deposition, such as metal or oxides, or localized surface modification. The results indicate that it will be possible, in the near future, to conceive and design devices for parallel analysis of biological samples made of arrays of nanopores differently functionalized, fabricated by standard lithographic techniques, with important applications in the field of molecular diagnosis.

1. Introduction

Single molecule sensing with nanopores is a rapidly developing field which exerts a special fascination on the scientific community, both for the potential revolutionary effect it can have on bioanalytics and diagnostics, and for its striking intrinsic interdisciplinary nature. Starting from the first papers mainly devoted to illustrate the properties of protein pores [1], much work has been done to realize engineered devices with specific characteristics and sensing abilities. Nowadays, the spectrum of proposed nanopore applications is quite large, most of them being based on electrophoretic current measurements during molecule translocation, i.e. on a simple functioning principle which does not need molecular labelling and optical detection. Nanopore sensing can thus provide a low cost, fast processing, and high throughput alternative to current DNA analysis and sequencing techniques.

The specific sensing mechanism merges Coulter counting and single current recording: the nanopore conductance is modulated during the passage of single molecules by steric or electrostatic effects, that is by the physical obstruction of the nano-channel and by the electrostatic interaction between the charge carried by the molecule and that present on the pore walls.

Nevertheless, nanopore properties can be finely tuned by introducing artificial binding and recognition sites or, generally speaking, by chemically modifying their surface properties [2, 3]. In this way it is possible to confer selectivity to the sensing process and to introduce novel biological and chemical functionalities. For example, biological pores have been engineered by amino acid replacement or substitution [4, 5] for stochastic sensing of metal ions, or by covalent attachment of oligonucleotides [6] and PEG chains [7] to probe complementarity of target DNA molecules or sense proteins, respectively. Non-covalent adaptors can also be used, hosted inside the protein channel, to allow the binding of analytes [8].

A similar approach has been recently applied in the case of artificial, solid state nanopores, which are more robust and stable than biological ones, but originally non-selective and chemically inert. For instance, the spontaneous chemisorption of thiols on Au and Ag surfaces was exploited to alter the surface charge of metal coated track-etched nanopores [9] and to attach various biochemical species to the nano-channel surface [10, 11], while oxide nanopores were principally modified by silanization [12–14] as a first activation step preceding the functionalization with amino-terminated molecules. An analogous 'bridge role' is played by carboxyl groups present on polymer nanopores [15, 16].

The current strategy to adjust or remove undesired properties has been to chemically modify silicon nitride nanopores: Chen *et al* used aluminium oxide deposition to reduce both the low frequency noise level and the cation selectivity [17], while Wanunu and Meller succeeded in controlling the pH response of the device by self-assembled organosilane molecule coating [18]. On the other hand, Nilsson *et al* [12] improved the control of SiN nanopore functionalization by performing local surface modification. Specifically, they were able to deposit a ring of silicon oxide just at the rim of the nanopore, which was then modified via silanization and subsequent single strand DNA attachment. Such engineered pores, both biological, like those studied in [6], and 'artificial' as in [13], actually constitute the basis for a novel kind of biosensor device for gene expression profiling: a current measurement allows us to analyse single molecule translocations through the functionalized nano-channel, distinguishing hybridization events between complementary target and probe molecules and identifying the eventual presence of single base mismatches. This translocation based mechanism can be truly sensitive and fast, requiring very small analyte quantities, and appearing as an appealing alternative to those founded on permanent blockage caused by biorecognition events [19, 20] or on monitoring of the noise [21–23] and rectification properties [24, 25] of the nanopore during interaction.

The present paper describes a simple and powerful approach for the production of a class of new biosensor devices based on bio-functionalized SiN nanopores [26–28] potentially able to detect different kinds of interactions between probe molecules, chemically attached to the pore, and target molecules. The great capability of this approach resides in the fact that a quite large pore (up to 50–60 nm) can be simultaneously activated and resized by bio-functionalization, to obtain selective single molecule sensing, without the need for further material deposition, such as metal or oxides, or localized surface modification.

The paper analyses the size reduction of the pore caused by single and double strand DNA (ssDNA, dsLNA) probe molecule attachment, and the peculiar electrical properties of the chemically modified nanochannel. In particular, the presence of the functionalization layer is verified by SEM imaging and detected as an increase in the electrical resistance, directly related to the decrease of the pore diameter. We also discuss the rectification of the current–voltage curve induced by the functionalization procedure and investigate the electrical noise and surface charge properties of the device.

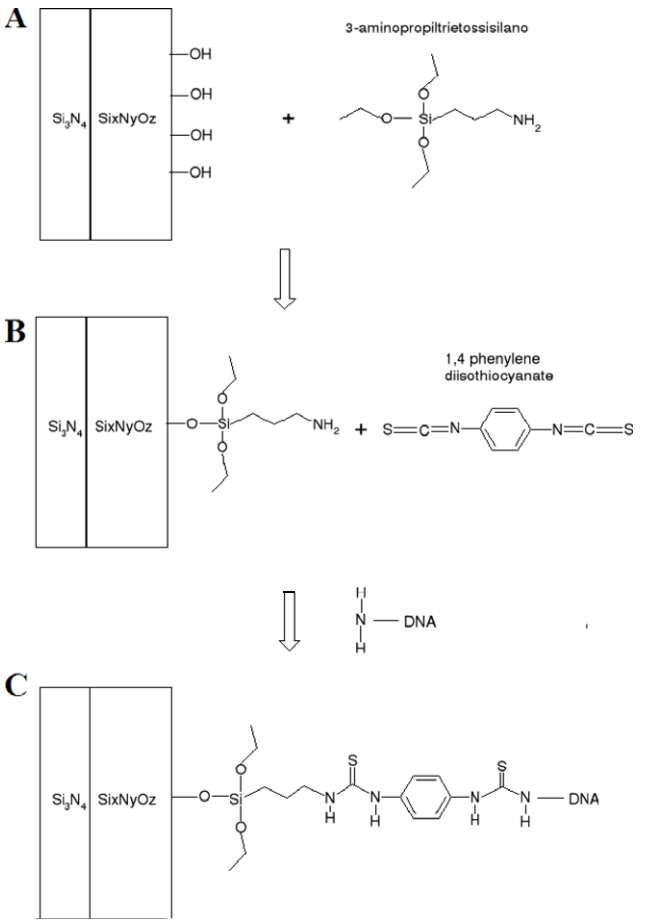

Figure 1. Scheme of the chemical functionalization procedure.

2. Experimental details

2.1. Nanopore fabrication

Nanopores with a 20 to 60 nm diameter were initially produced on a free-standing SiN insulating membrane by using a CrossBeam® model 1540XB Zeiss workstation that combines an ultra-high resolution scanning electron microscope (UHRSEM) and a focused ion beam (FIB). The membrane was obtained by depositing a thin (20 nm thick) silicon nitride (SiN) film on a 300 μm thick Si substrate, and anisotropically etching the Si side of the chip to expose a squared area 80 $\times$ 80 μm^2 large. By realizing a cross section of the FIB fabricated nanopores we verified that the produced channels usually show an asymmetric conical geometry, slightly enlarged on the SiN membrane side [26].

2.2. Chemical functionalization of nanopores

The SiN membrane containing the nanopore was chemically functionalized by following a three-step procedure (figure 1) [27]. Firstly, the entire membrane was activated for 1 h with 3-aminopropyltriethoxysilane (20% V/V in ddH_2O) that links to the $-$OH groups of the native silicon oxide layer present on the silicon nitride surface (figure 1(A)). The second step involves a treatment with 1,4-phenylenediisotiocyanate (0.5% P/V in dimethyl-sulfoxide) cross-linker for 5 h

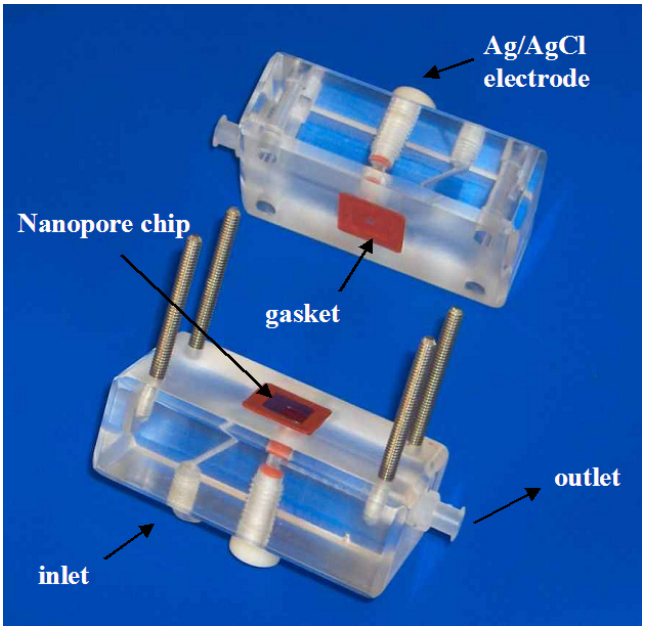

Figure 2. Picture of the cell used for the electrical measurements and made of two facing Plexiglas chambers filled with ionic solution by means of a microfluidic system (connected to the inlet and outlet on both sides). The lodgings of the chip and of the Ag/AgCl electrodes are indicated by arrows, together with the used seal gaskets.

(This figure is in colour only in the electronic version)

followed by two washes in dimethyl-sulfoxide and two washes in double distilled water (figure 1(B)). The third step consists of over-night treatment at 37 °C with 100 nM amino-modified DNA in ddH_2O pH 8–9 (figure 1(C)). Finally, the substrate was de-activated by two washes (30 min each) with 28% ammonia solution followed by two washes with ddH_2O (15 min each).

Both ssDNA and dsLNA are linked to such an activation layer thanks to the amino groups. As ssDNA probe we used an amino-modified 45-mer oligonucleotide (Eurofins MWG Operon, Germany) corresponding to a GAPDH (glyceraldehyde-3-phosphate dehydrogenase) 5′-GCC AAA AGG GTC ATC ATC TCT GCC CCC TCT GCT GAT GCC CCC ATG-3′ sequence [26–28]. The used dsLNA is a decoy oligodeoxynucleotide (ODN) containing locked nucleic acids. Locked nucleic acids (LNA) are nucleoside analogues containing a methylene linkage between the 2′-oxygen and 4′-carbon of the ribose ring and constrain the sugar moiety, in LNA decoys, in an induced conformational change produced in the helical geometry of the decoy sequence varying with the extent and position of LNA substitution. The lock is positioned at the terminal ends of a decoy and it confers protection against DNase I digestion probably perturbing the interactions between the enzyme and target DNA [29]. The utilized decoy contains the consensus sequence for NF-kB, a transcription factor involved in numerous cellular functions with sequence 5′-*TA* AGA GGG AAA TTC CGG GAA ATT CCT AC *AT*-3′. The underlined nucleotides include LNA and the sense strand of the ODN is amino-modified by a C6 bridge. Both the strands were purchased from Sigma-Proligo.

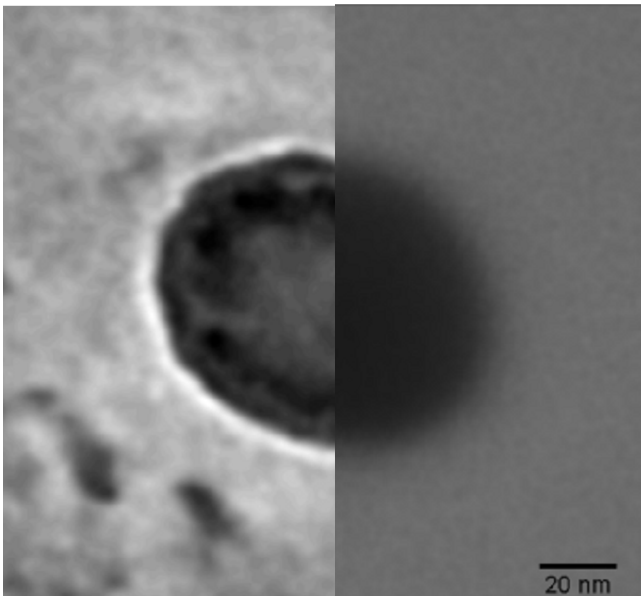

Figure 3. SEM images of the same nanopore before (half image on the right) and after (half image on the left) the functionalization procedure: the presence of the organic layer can be seen as a jagged edge, with a mean thickness of about 10–20 nm.

2.3. Current measurements

To realize the current measurements the nanopore chip was mounted between two facing Plexiglas chambers filled by means of a microfluidic system (figure 2) with 300 μl of filtered KCl 1 M ionic solution buffered at pH 8 with 10 mM HEPES. Two Ag/AgCl electrodes were used to apply a voltage bias and to collect the ion current by means of a patch clamp amplifier (Axopatch 200B, Axon Instruments, 1–200 kHz sampling rate, amplifier internal low-pass four-pole Bessel filter set at 10 kHz). The entire apparatus was finally placed in a double Faraday cage enclosure on an anti-vibration table to reduce electrical and mechanical noise.

3. Results and discussion

The chemical functionalization of nanopores causes an evident resizing, i.e. a shrinking of the diameter, which is directly related to the length of the used probe molecules [26–28]. This size reduction can be visualized by comparing SEM images of the same nanopore before (figure 3, half image on the right) and after (figure 3, half image on the left) the functionalization procedure; the presence of the organic layer can be seen as a jagged edge, with a mean thickness of about 10–20 nm which is compatible with the length of the 45-mer oligonucleotides attached to the SiN surface.

The effect of the nanopore obstruction due to the chemical activation can be also detected as an increase in the electrical resistance (R) of the modified nanopore. Figure 4 presents, as an example, typical voltage–current (I/V) curves measured in KCl 1 M on the same chip, before and after ssDNA (figure 4(A), left) and dsLNA (figure 4(B), right) molecule binding. In both cases a large and stable enhancement of the

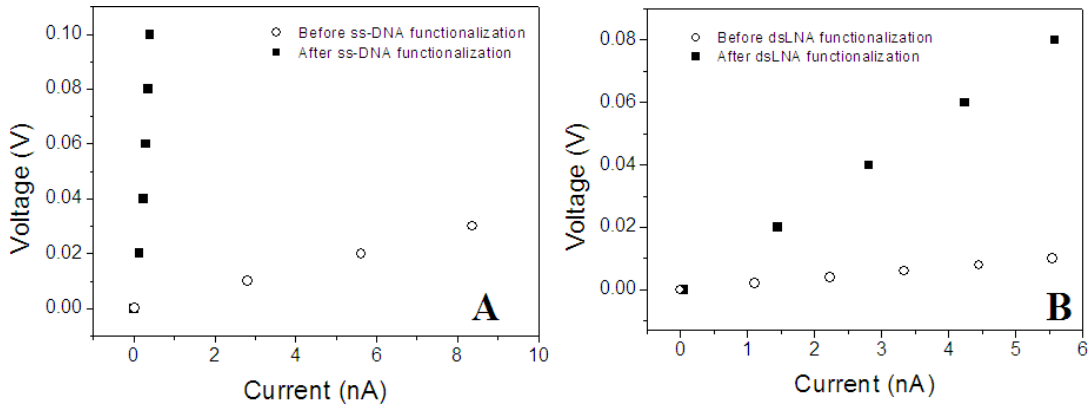

Figure 4. Typical voltage–current (I/V) curves measured in KCl 1 M on the same chip before (open circles) and after (solid circles) ssDNA ((A), left) and dsLNA ((B), right) molecule binding.

initial pore resistance is obtained. A linear fit of the curves allows an estimation of R, which passes from 3.5 to 245 MΩ for ssDNA functionalization, and from 1.8 to 14.5 MΩ for dsLNA functionalization. By making a constant diameter approximation for the nanometric channel produced by FIB milling, these data can be used to evaluate the reduction of the so-called 'effective radius', $r_{\mathrm{eff}} = \sqrt{l/(c\pi R)}$, where c is the conductivity of the used ionic solution ($c \sim 10$ S m^{-1} for KCl 1 M), and l is the 20 nm channel length corresponding to the SiN membrane thickness. The measured variation in R therefore corresponds to an effective radius reduction of about 11.9 nm and 12.2 nm for, respectively, ssDNA and dsLNA functionalization. Both values are compatible with the expected linear dimension of the linked probe molecules and the results of SEM imaging. Nevertheless, this kind of electrical determination, although useful for a rapid analysis of the chemically modified pore, is not completely accurate, because it does not consider the possible geometric asymmetry of the pore and the presence, on the channel walls, of the surface charge carried by the probe molecules. This is evident by looking at the data reported in figure 5, depicting the values of the effective radius reduction of ssDNA and dsLNA functionalized nanopores as a function of the initial r_{eff}; the shrinking of the nanopore appears to linearly decrease with the starting radius. We speculate that this unexpected behaviour is a consequence of an overestimation of the chemically modified channel dimension. The r_{eff} definition, in fact, does not consider the presence of an additional contribution to the nanopore conductance coming from the presence of a net surface charge σ on the pore walls. As explained in [30], the nanoscale fluidic channel conductance G can be written as the sum of two contributions; a bulk term, which is proportional to the concentration of the ionic solution, and a surface term, due to the formation of the so-called 'electric double layer' (EDL) of mobile counterions [31] screening σ, which dominates the transport phenomena at very low salt concentration ($<10^{-3}$ M):

$$G = \frac{\pi}{4}\frac{d_{\mathrm{pore}}^2}{l}\left[A \times \mathrm{conc} + \left(\frac{B}{d_{\mathrm{pore}}}\right)\sigma\right]. \qquad (1)$$

In expression (1), A and B are constant terms containing the bulk ion mobilities for K^+ and Cl^- ions, while d_{pore} is the 'real' nanopore diameter. When the radius of the channel is very small, the surface contribution becomes substantial and causes an increase of the measured conductance with respect to that predicted for a purely bulk process. As a consequence, the effective radius deduced from the measured R value is larger, i.e. the estimated shrinking is smaller than the real one.

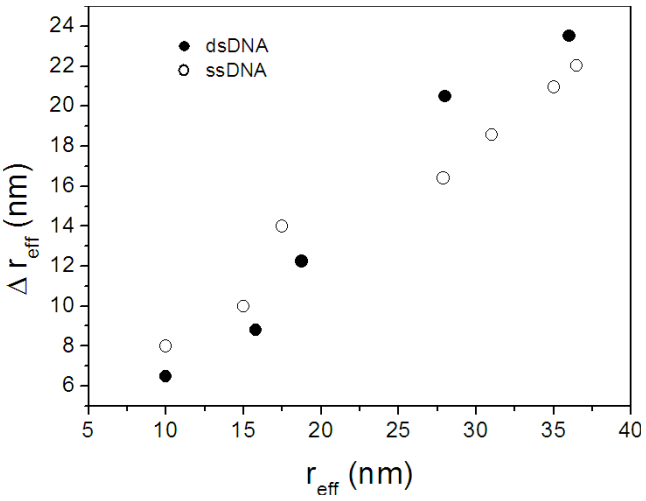

Figure 5. Effective radius reduction Δr_{eff} following the ssDNA and dsLNA functionalization, deduced by the resistance measurements in KCl 1 M, as a function of the initial r_{eff}.

A confirmation of our assumption is given by the data presented in figure 6. The figure reports the behaviour of the conductance G normalized to its $G_{1\,\mathrm{M}}$ value measured at 1 M as a function of the ionic concentration. In particular, the data relate to the regime of very low ionic concentration ($<10^{-4}$ M) at which, as mentioned above, surface effects become more important. The measurements were performed on three ssDNA functionalized nanopores, having different effective radius, from 3.9 to 17 nm, and show that not only $G/G_{1\,\mathrm{M}}$ is independent, in this regime, of the salt concentration, but it also significantly rises for decreasing effective diameters.

This trend is qualitatively described by the low concentration limit of expression (1) that can be written as:

$$\frac{G}{G_{1\,\mathrm{M}}}(\mathrm{conc} \to 0) \approx \frac{B\sigma}{Ad_{\mathrm{pore}} + B\sigma}. \qquad (2)$$

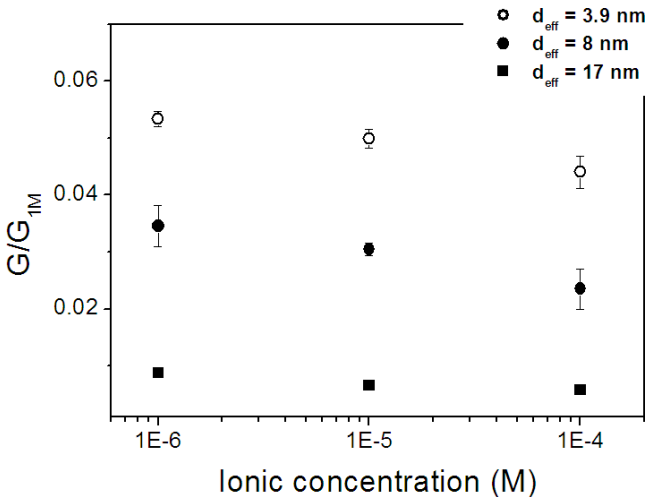

Figure 6. Behaviour of the conductance G normalized to its $G_{1\,\mathrm{M}}$ 'bulk' value measured at 1 M (i.e. at high salt concentration) as a function of the ionic concentration. The presented data relate to the regime of very low ionic concentration ($<10^{-4}$ M) at which surface effects become important. The measurements were performed on three ssDNA functionalized nanopores, having different effective radius, from 3.9 to 17 nm.

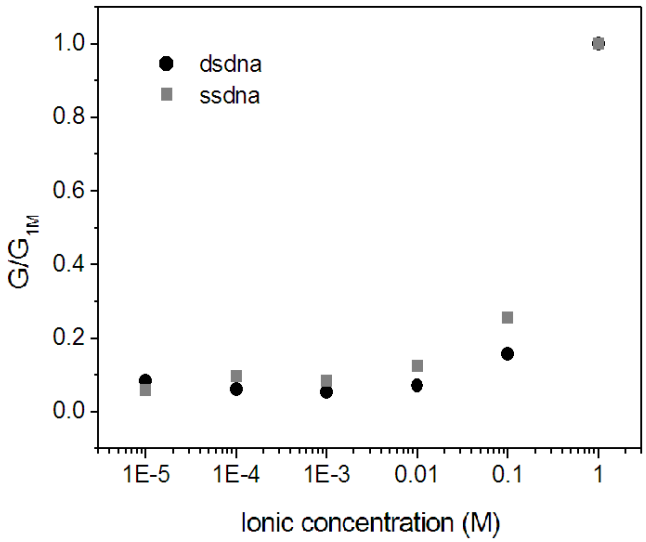

Figure 7. Behaviour of the conductance G normalized to its $G_{1\,\mathrm{M}}$ 'bulk' value at different ionic concentrations ranging from 1 M to 10^{-5} M obtained on two nanopores functionalized with ssDNA (black circles) and dsLNA (grey squares) probe molecules. The two nanopores have similar effective diameters, 8 and 13 nm, respectively.

By approximating d_{pore} with the effective diameter, expression (1) can be used to directly fit the $G/G_{1\,\mathrm{M}}$ data, in order to evaluate σ. Figure 7 compares the $G/G_{1\,\mathrm{M}}$ values at different ionic concentrations (ranging from 1 to 10^{-5} M) obtained on two nanopores functionalized with ssDNA and dsLNA probe molecules, with effective diameters equal to 8 and 13 nm, respectively. Interestingly, the two plots are almost superposed, i.e. the two nanopores have similar surface charges of about 45 mC m^{-2}. By considering the slightly different radius of the two pores, and the fact that dsLNA carries a double charge with respect to ssDNA, we estimated that 12 single strand and 10 double strand probe molecules are present on the channel's surface.

The I/V curve appears asymmetric for positive and negative polarities, revealing another intriguing characteristic of chemically modified nanopores. In general, we found that this rectification effect reduces with decreasing channel lengths (i.e. membrane thickness) [26], but it can become very evident for very small functionalized nanopores. This is demonstrated in figure 8, showing the I/V curve measured in KCl 1 M on the same 20 nm thick nanopore chip before (open circles) and after (solid circles) the functionalization with ssDNA. The initial electrical resistance of the bare SiN nano-channel, as derived by a linear fit of the data, is $R \sim 3.6$ MΩ, corresponding to an effective radius of about 13.5 nm. The functionalization with 15.3 nm long oligonucleotides is then able to almost completely close the nanopore. In this condition the I/V curve is strongly rectified after the chemical modification. In particular, we obtained a resistance $R \sim 36$ MΩ and $R \sim 256$ MΩ for, respectively, a negative and positive voltage bias.

Similar ionic current rectification effects have been observed for both biological and synthetic nano-channels, and several models have been developed to qualitatively explain this behaviour [32]. Asymmetric effects in the I/V curve are ascribed to an overall system symmetry breaking, i.e. to

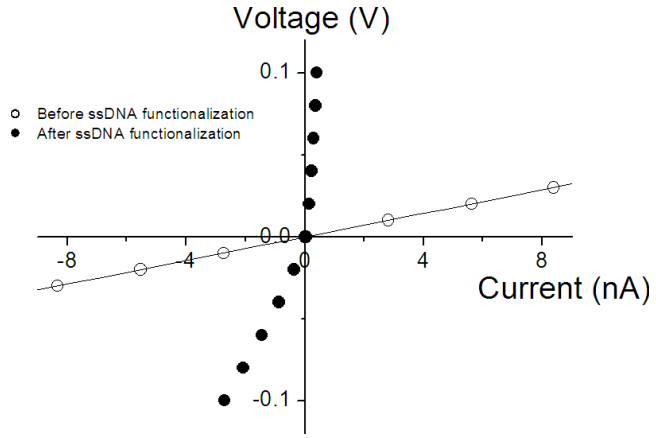

Figure 8. I/V curve measured in KCl 1 M on the same 20 nm thick nanopore chip before (open circles) and after (solid circles) the functionalization with ssDNA.

the establishment of a preferential direction for the ion flux. Several possible causes were identified for the rectification of the voltage–current curve, most of them having an electrostatic origin:

(1) *Ion concentration gradient along the pore* [33, 34]. As demonstrated in [34] the rectifying effect appears when the ion concentrations on the two baths are set up to induce EDL overlap at the single side of the nano-channel, producing asymmetric cation/anion ratios or built-in potentials at the two entrances.

(2) *Surface charge gradient*, which can be induced by a pH variation [35, 36] or by asymmetric functionalization [15, 37], with the resulting system that behaves as a 'nanofluidic diode'.

(3) *Geometric asymmetry of a uniformly charged channel* [9, 38]. In this case the resistance is higher when

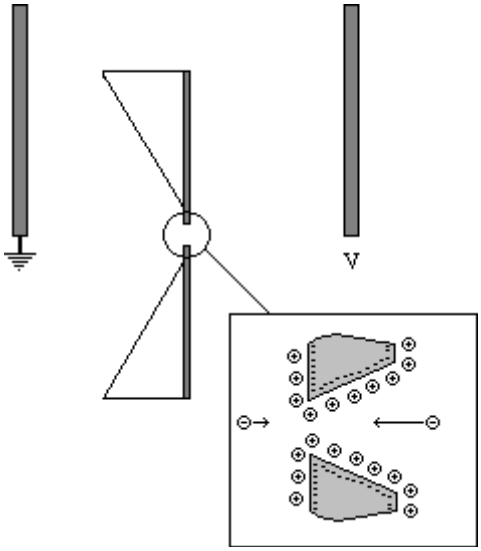

Figure 9. Sketch of the configuration used to obtain the measurements of figure 8, with an inset representing a magnification of the membrane to clarify the channel shape and orientation.

the negative electrode (cathode) is placed on the narrower side of the channel, and the rectification effect can only be revealed for a confined channel geometry comparable with the EDL. In other words the channel radius and the salt concentration must be sufficiently low to cause surface effects to become important.

(4) *Electro-mechanical effects* [11, 39]. Chemical functional groups and charged molecules attached at the entrance of the pore can move and insert into and out of the channel, contributing to the voltage dependence of the pore's diameter.

Actually, nanopores produced by FIB drilling appear slightly enlarged on the side on which the Ga^+ ions impinge during the fabrication process [26], thus acquiring a conical shape. Figure 9 presents a sketch of the configuration used to obtain the measurements of figure 8, with an inset representing a magnification of the membrane. Therefore, our results agree with those reported in [9, 38]; the resistance is higher when the cathode is placed on the narrower side of the nano-channel, i.e. for positive bias, and the asymmetry of the I/V curve is only evident after the functionalization procedure, which sufficiently reduces the effective diameter of the nanopore. The electro-mechanical effects due to the presence of the probe molecules (especially those linked to the narrower tip of the channel [39]) and the surface charge gradient associated with incomplete probe coverage of the pore walls, should also be taken into account.

Finally, we investigated the electrical noise properties. Solid state nanopores usually exhibit, during current measurements, a lower signal to noise ratio with respect to biological ones, due to the presence of enhanced low frequency conductance fluctuations ($1/f$ and excess white noise [39, 40]). Some authors succeeded in reducing the $1/f$ flicker noise contribution by chemically modifying the channel surface. In [17] the atomic deposition of Al_2O_3 on the SiN membrane allowed the sensing characteristics of the pore to be strongly

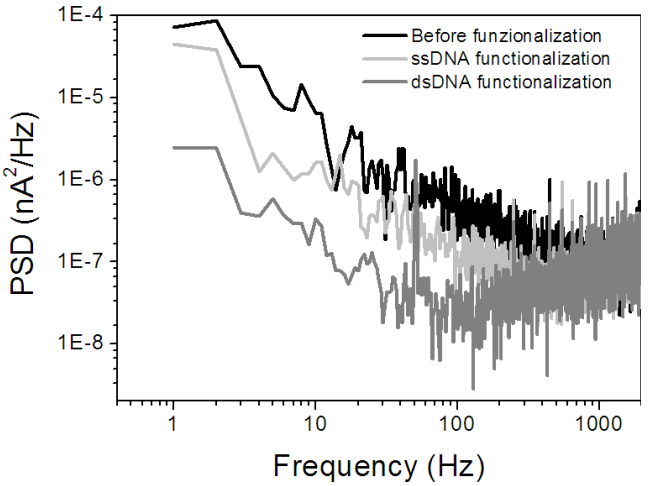

Figure 10. PSD of current traces collected at the same constant voltage of 110 mV before (black line) and after the functionalization with both ssDNA (light grey line) and dsLNA (dark grey line) probe molecules.

enhanced by greatly reducing the noise level. We tested the nanopores' characteristics by analysing the power spectral densities (PSD) of current traces collected at the same constant voltage of 110 mV before and after the functionalization with both ssDNA and dsLNA probe molecules (200 kHz sampling rate, amplifier internal low-pass four-pole Bessel filter set at 10 kHz). The results show (figure 10) a sensible reduction of the low frequency noise after the chemical modification of the nano-channel. Notably, the reduction is more pronounced for dsLNA attachment. Even though much study is needed to better understand the origin of this surface property tuning effect, we believe that this finding could play a great role in establishing improved single molecule sensing characteristics of our nanopore based biosensor device.

4. Conclusions

We have presented electrical characterization of chemically modified FIB fabricated nanopores, analysing the size shrinking produced by probe molecule attachment on the channel walls and the surface modification induced by the functionalization procedure, and showed specific rectification and electrical noise reduction effects. We demonstrated that, by starting from bare SiN nanopores having an effective diameter of 20–60 nm, it is possible to obtain a final device with dimensions compatible with single molecule sensing applications (2–6 nm) and potentially selective for different kinds of interactions between probe and target molecules. This type of hybrid biosensor, which could be integrated into more complex microfluidic devices and labs-on-a-chip, promises to have important applications in the field of molecular diagnosis.

Acknowledgments

This work has been supported by Ministero dell'Università e della Ricerca (MIUR), Italy, with the FIRB 2003 National Project *Nanomed*. We thank Fondazione Bruno Kessler, FBK,

for the Si/SiN chip fabrication and ElbaTech S.r.l. for the microfluidic cell construction.

References

[1] Kasianowicz J J, Brandin E, Branton D and Deamer D W 1996 *Proc. Natl Acad. Sci. USA* **93** 13770
[2] Howorka S and Siwy Z 2009 *Chem. Soc. Rev.* **38** 2360–84
[3] Gyurcsanyi R E 2008 *Trends Anal. Chem.* **27** 627–39
[4] Ausubel F M, Brent R, Kingston E, Moore D D, Seidman J G, Smith J A and Struhl K 2008 *Current Protocols in Molecular Biology* (New York: Wiley)
[5] Xie H, Braha O, Gu L Q, Cheley S and Bayley H 2005 *Chem. Biol.* **12** 109–20
[6] Howorka S, Cheley S and Bayley H 2001 *Nat. Biotechnol.* **19** 636–9
[7] Movileanu L, Howorka S and Braha O 2000 *Nat. Biotechnol.* **18** 1091
[8] Gu L Q, Braha O, Conlan S, Cheley S and Bayley H 1999 *Nature* **398** 686–90
[9] Siwy Z, Heins E, Harrel C C, Kohli P and Martin C R 2004 *J. Am. Chem. Soc.* **126** 10850–1
[10] Siwy Z, Trofin L, Kohli P, Baker L A and Martin C R 2005 *J. Am. Chem. Soc.* **127** 5000–1
[11] Harrel C C, Kohli P, Siwy Z and Martin C R 2004 *J. Am. Chem. Soc.* **126** 15646–7
[12] Nillson J, Lee J R I, Ratto T V and Letant S E 2006 *Adv. Mater.* **18** 427–31
[13] Iqbal S M, Akin D and Bashir R 2007 *Nat. Nanotechnol.* **2** 243–8
[14] Kim Y R *et al* 2007 *Biosens. Bioelectron.* **22** 2926–31
[15] Vlassiouk I and Siwy Z S 2007 *Nano Lett.* **7** 552–6
[16] Ali M, Ensinger W, Neumann R and Schiedt B 2007 *GSI Annual Report 2006* vol 1, p 323
[17] Chen P, Mitsui T, Farmer D B, Golovchenko J, Gordon R G and Branton D 2004 *Nano Lett.* **4** 1333–7
[18] Wanunu M and Meller A 2007 *Nano Lett.* **7** 1580
[19] Gyurcsanyi R E, Vigassy T and Pretsch E 2003 *Chem. Commun.* 2560–1
[20] Vlassiouk I, Takmakov P and Smirnov S 2005 *Langmuir* **21** 4776–8
[21] Bezrukov S M, Vodyanoy I and Parsegian V A 1994 *Nature* **370** 279–81
[22] Bezrukov S M and Kasianowicz J J 1997 *Eur. Biophys. J.* **26** 471–6
[23] Kasianowicz J J, Burden D L, Han L C, Cheley S and Bayley H 1999 *Biophys. J.* **76** 837–45
[24] Ali M, Bayer V, Schiedt B, Neumann R and Ensinger A 2008 *Nanotechnology* **19** 485711
[25] Wang J and Martin C R 2008 *Nanomedicine* **3** 13–20
[26] Mussi V, Fanzio P, Repetto L, Firpo G, Scaruffi P, Stigliani S, Tonini G P and Valbusa U 2010 *Nanotechnology* **21** 145102
[27] 2009 DNA-functionalized silicon nitride nanopores for gene expression profiling *Patent No.* RM2009A000450, 4th (Sept.)
[28] Mussi V, Fanzio P, Repetto L, Firpo G, Valbusa U, Scaruffi P, Stigliani S and Tonini G P 2008 *Superlatt. Microstruct.* **46** 59
[29] Crivelli R, Bianchi M, Gentilini L, Palma L, Sorensen M D, Bryld T, Babu R B, Arar K, Wengel J and Magnani M 2004 *Nucl. Acids Res.* **32** 1874–85
[30] Smeets R M M, Keyser U F, Krapf D, Wu M Y, Dekker N H and Dekker C 2006 *Nano Lett.* **6** 89
[31] Schoch R B, Han J and Renaud P 2008 *Rev. Mod. Phys.* **80** 839–83
[32] Siwy Z 2006 *Adv. Funct. Mater.* **16** 735
[33] Siwy Z and Fulinski A 2002 *Phys. Rev. Lett.* **89** 198103
[34] Cheng L and Guo L J 2007 *Nano Lett.* **7** 3165–71
[35] Fulinski A, Kosinska I and Siwy Z 2004 *Europhys. Lett.* **67** 683
[36] Wang L, Guo W, Xie Y B, Wang X W, Xue J M and Wang Y G 2009 *Radiat. Meas.* **44** 1119–22
[37] Vlassiouk I, Kozel T R and Siwy Z S 2009 *J. Am. Chem. Soc.* **131** 8211–20
[38] Siwy Z S and Fulinski A 2004 *Am. J. Phys.* **72** 567
[39] Hofler L and Gyurcsanyi R E 2008 *Electroanalysis* **20** 301–7
[40] Hoogerheide D P, Garaj S and Golovchenko J A 2009 *Phys. Rev. Lett.* **102** 256804